J Fluoresc (2015) 25:1215–1223
DOI 10.1007/s10895-015-1608-z

ORIGINAL ARTICLE

Physicochemical Characterization and In Vitro Cytotoxic Effect of 3-Hydroxyflavone in a Silver Nanoparticles Complex

Mariana Voicescu[1] · Oana Craciunescu[2] · Lucia Moldovan[2] · Mihai Anastasescu[1] · Daniel G. Angelescu[1] · Valentin S. Teodorescu[3]

Received: 16 March 2015 / Accepted: 30 June 2015 / Published online: 24 July 2015

Abstract The aim of this work was to characterize the physico-chemical properties of 3-hydroxyflavone (3-HF) in a silver nanoparticles complex (SNPs) using UV–vis and Fluorescence spectroscopy, Atomic Force Microscopy (AFM) and Transmission Electron Microscopy (TEM) analysis. One also evaluated its effect on the cell viability and morphology of L929 mouse fibroblast cells in vitro. The contribution of the carrier protein, Bovine Serum Albumin (BSA) to 3-HF properties has also been investigated. 3-HF in BSA/SNPs systems presented no cytotoxic effect in L929 mouse fibroblast cells at any of the tested concentrations. The results are discussed with relevance to the oxidative stress process.

Keywords Flavones · Silver nanoparticles · Proteins · Fluorescence · Cytotoxicity

Introduction

Flavones and related compounds of the flavonoid group in plant poly-phenolic derivatives perform various therapeutic properties such as: antioxidant, antiradical, angioprotective, making them effective agents against cancers, tumors, cardiac problems, inflammations, allergies, Acquired Immune Deficiency Syndrome [1–6]. Other remarkable types of activity of flavones are based on their dual fluorescence behavior, known as systems exibiting intramolecular excited state proton transfer, ESIPT, for exploring the structure, function, dynamics, interactions and microenvironment in biological systems like proteins [7–12].

Several biological and biomedical applications are based on the use of the metalic nanoparticles [13–15], with a special attention to the silver nanoparticles (SNPs) and their use in the treatment of burn wounds [16–22]. Studies on the SNPs syntheis and their antibacterial and antimicrobial activity show that SNPs act as an effective bactericide against gram positive bacteria such as *Escherichia coli*, *Pseudomonas aeruginosa* and *Staphylococcus aureus* [23–27]. Applications of SNPs in clinical medicine [28, 29] and more recently, aspects concerning mechanisms of nanoparticles-induced oxidative stress and toxicity [30], have been reported. In the last case, changes in structural and physico-chemical properties of nanoparticles can lead to changes in biological activities including reactive oxygen species (ROS) generation, one of the most frequently reported nanoparticles-associated toxicities [30]. Moreover, oxidative stress induced by engineered nanoparticles is due to cellular factors (such as particle surface, size, composition, the presence of the metals), while cellular responses (such as mitochondrial respiration, nanoparticles-cell interaction, the immune cell activation) are responsible for ROS-mediated damage [30]. Thus, the oxidative stress is a key determinant of nanoparticle-induced injury; A characterisation of the ROS response resulting from nanoparticles is needed [30]. Also, studies regarding the cytotoxicity of flavonoid compounds (apigenin, eriodictyol, 3-hydroxyflavone, kaempherol, luteolin, naringenin, quercetin, rutin, taxifolin), towards cultured normal human cells, with cytotoxicity in a dose-dependent manner, have been reported [31].

✉ Mariana Voicescu
voicescu@icf.ro

[1] Institute of Physical Chemistry "Ilie Murgulescu" of the Romanian Academy, Splaiul Independentei 202, 060021 Bucharest, Romania

[2] National Institute of R&D for Biological Sciences, Splaiul Independentei 296, 060031 Bucharest, Romania

[3] Institute of Atomic Physics, National Institute of Materials Physics, Magurele 077125, Romania

This work is an extension of our recent study [32] and aims to evaluate the effect of 3-Hydroxyflavone (3-HF) in a silver nanoparticles complex (SNPs) on the cell viability and on the cell morphology of L929 mouse fibroblast cells in vitro. The contribution of the carrier protein, Bovine Serum Albumin (BSA), to 3-HF properties has been also investigated. UV–vis and Fluorescence spectroscopy, Atomic Force Microscopy (AFM), Transmission Electron Microscopy (TEM) analysis, have been used. The results are discussed with relevance to the oxidative stress process.

Experimental

Materials

3-Hydroxyflavone (3-HF), with the molecular structure presented in Scheme 1, was purchased from Sigma and used without further purification. Stock solution of 3.6 mM was prepared in methanol (of spectrophotometric grade, purchased from Sigma, 99 %). As a function of experimental method, aliquots from the stock solution were added to the working sample to reach the final concentration in the range of 6×10^{-5} M$\div1.2\times10^{-4}$ M. Bovine Serum Albumin (BSA) was purchased from Merck, Darmstadt, and in a typical experiment, the final working concentration was in the range of $2.06\div6\times10^{-6}$ M.

The silver source, silver nitrate ($AgNO_3$, purity 99.99 %) and the reducing agent, sodium borohydride ($NaBH_4$, purity 99.8 %) were purchased from Sigma-Aldrich. *Ag (0) nanoparticles (SNPs)* were synthesized according to ref. [33], by adding under vigorous stirring appropriate aliquots of 1 mM $AgNO_3$ aqueous solution to an aqueous solution containing $NaBH_4$, to their final concentrations of 0.1 mM $AgNO_3$ and 7 mM $NaBH_4$, respectively.

A mouse fibroblasts cell line (NCTC clone L929) was purchased from ECACC (Sigma-Aldrich, Germany). Minimum Essential Medium (MEM), fetal calf serum (FCS), L-glutamine, trypsin (E.C. 3.4.21.4), ethylenediaminetetra acetic acid disodium salt (EDTA), 3-(4,5-dimethylthiazol-2-yl)-2,5-diphenyltetrazolium bromide (MTT) and all other chemicals of analytical grade were purchased from Sigma-Aldrich Chemicals (Germany).

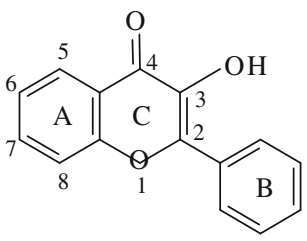

3-Hydroxyflavone

Scheme 1 Molecular structure of 3-hydroxyflavone

Methods and Apparatus

The absorption measurements were recorded using a Perkin Elmer, Lambda 35, UV–vis Spectrometer at a scan rate of 480 nm/min with a spectral resolution of 1 nm.

Transmission electron microscopy specimens were prepared by placing droplets of the aqueous solution containing 3-HF/SNPs complex onto carbon-coated TEM grid and subsequently letting evaporation of the solvent under ambient conditions. The as-synthesized nanoparticles were visualized using a transmission electron microscope model JEM 200CX equipped with a KeenView CCD camera and operating at 120 kV. Size analysis involved more than 100 nanoparticles from several snapshots.

The fluorescence emission and excitation spectra were recorded with a Jasco FP-6500 Spectrofluorometer, using 3 nm bandpass for the excitation and the emission monochromators, the detector response of 1 s, data pitch of 1 nm, the scanning speed of 100 nm/min. The excitation wavelengths were 365 nm and 280 nm for 3-HF emission and Tryptophan (Trp) emission, respectively.

Atomic force microscopy (AFM) measurements were carried in the non-contact mode, with an XE-100 apparatus from Park Systems (2011), using ultra-sharp tips (<8 nm tip radius; PPP-NCHR type from Nanosensors™). The topographical 2D and 3D AFM images were taken over the area of 1×1 μm^2, and the horizontal line by line flattening was used as planarization method for displaying purpose and subsequent statistical data analysis, including the calculation of the root mean square (RMS) roughness using the Image Processing Program (XEI – v.1.8.0) developed by Park Systems. For AFM analysis, the sample deposition has been done on quartz plates, with the molar ratio 3-HF:BSA=10:1 in the SNPs complex.

Cell Culture, Growth Conditions and Treatment Mouse fibroblasts from NCTC clone L929 cell line were grown in T75 flasks in MEM supplemented with 10 % FCS, 2 mM L-glutamine and 1 % mixture of antibiotics. Cultures were maintained in an incubator with humidified atmosphere of 5 % CO_2 and 95 % air, at 37 °C. For experiments, cells were harvested from subconfluent cultures using 0.25 % trypsin-EDTA solution and were re-suspended in fresh serum-supplemented growth medium before plating. The cell suspension was seeded in 24-well culture plates, at a density of 5×10^4 cells/well and incubated in a humidified 5 % CO_2 atmosphere, at 37 °C, to allow cell adhesion. After 18 h of incubation, cells were treated with SNPs (0.9 μM); 3-HF (1.2×10^{-4} M)/SNPs and 3-

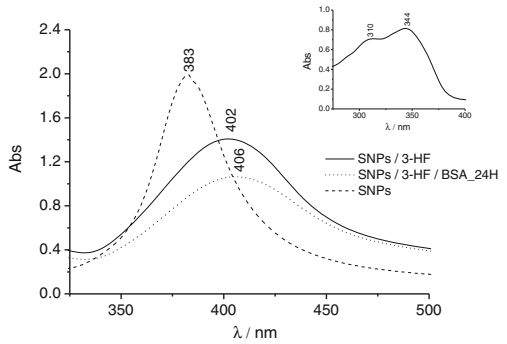

Fig. 1 UV–vis absorption spectra of the SNPs/3-HF/BSA system. *Inset* shows the absorption spectrum of 3-HF/BSA system. The concentration of 3-HF is 6×10^{-5} M. The concentration of BSA protein is 6×10^{-6} M

HF/BSA (2.06 μM)/SNPs, respectively, using 1.56÷50 μL of reaction mixture in 500 μL culture medium. The plates were incubated at 37 °C, in standard conditions of cultivation, for 24 and 48 h, respectively.

Cell Viability Assay At the end of the treatment, in vitro cytotoxicity of the samples was evaluated by the direct contact method, according to SR EN ISO 10993-5, using MTT assay [34]. Briefly, the medium was harvested after 24 and 48 h of cultivation, respectively. Fresh medium containing MTT solution, in a 10:1 (*v/v*) ratio was added and the plates were incubated at 37 °C, for 3 h. After incubation, the solution was removed, 500 μl isopropanol were added to each well and the plate was gently shaken on a platform, for 3 h, to dissolve the formazan crystals. The colored solution was transferred to another 96-well plate and the optical density (OD) was read at 570 nm, using a Sunrise microplate reader (Tecan, Austria). The results of triplicates were expressed as mean±standard deviation (SD). Cells cultured with complete culture medium served as control, considered 100 % viable.

Cell Morphology Cells grown in the presence of samples for 48 h were fixed in methanol, stained with Hematoxylin-Eosin and visualized at an AxioObserver D1 microscope, equipped with an AxioCam MR3 digital camera (Carl-Zeiss, Jena, Germany).

Statistics Data were expressed as mean±SD (n=3). Statistical analysis of the data was performed using the paired Student's t-test, on each pair of interest. Differences were considered statistically significant at $p<0.05$.

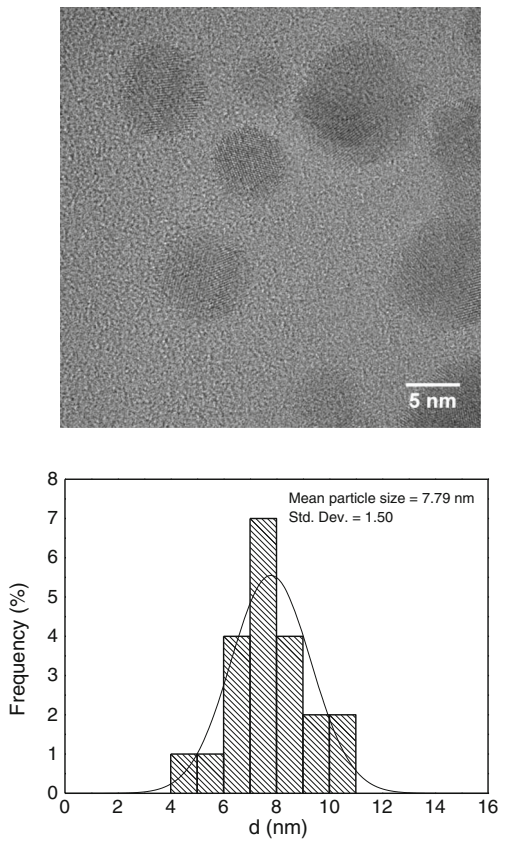

Fig. 2 Representative TEM images of 3-HF/SNPs complex with the particle size distribution and Gaussian best-fit of the SNPs; the concentration of 3-HF is 6×10^{-5} M

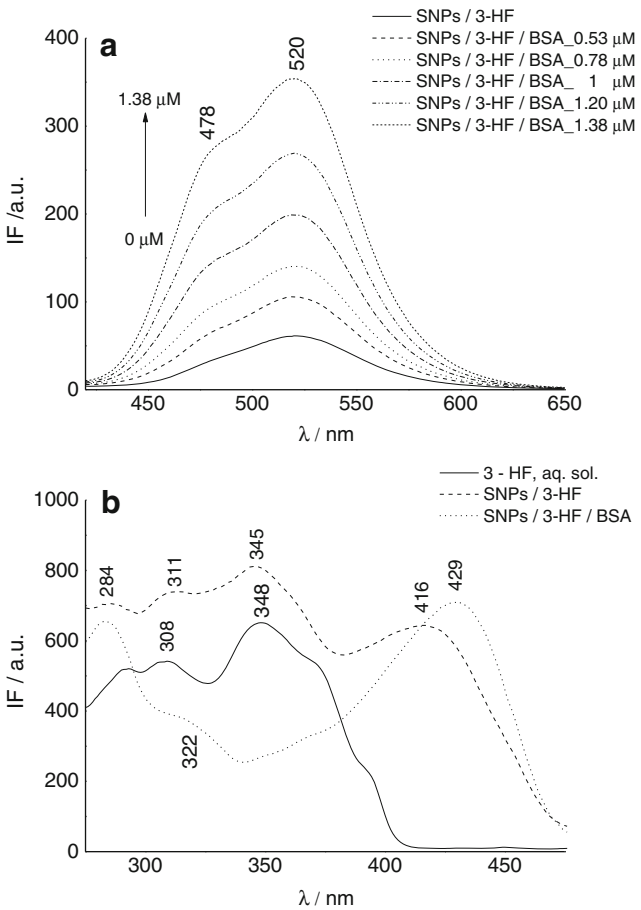

Fig. 3 Fluorescence emission (**a**) and excitation (**b**) spectra of SNPs/3-HF/system in the presence of various concentration of BSA; λ_{ex}=365 nm; λ_{em}=530 nm; [3-HF]=6×10^{-5} M

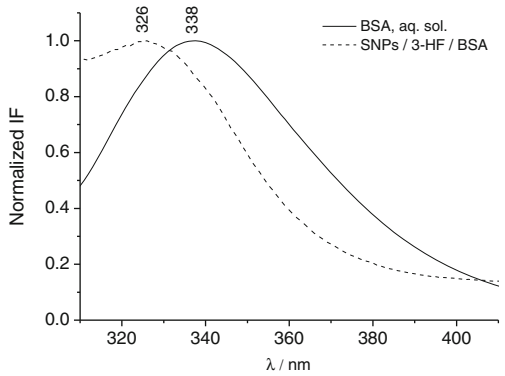

Fig. 4 Normalized Trp fluorescence emission of SNPs/3-HF/BSA system in direct comparison with Trp emission of aqueous solution of BSA; [3-HF]=6×10^{-5} M, [BSA]=1.61 μM, λ_{ex}=280 nm

Results and Discussion

Absorption Measurements

Structural characterization of the 3-HF in BSA/SNPs systems is shown in Fig. 1. The absorption spectrum of 3-HF in a SNPs complex as well as in the BSA/SNPs complex shows a surface plasmon absorption band with a maximum at 402 and 406 nm respectively, in direct comparison with the plasmon absorption band of the bare SNPs, at 383 nm. For 3-HF/BSA/SNPs system, the broad plasmon absorption band at 406 nm corresponds to adsorbed BSA protein on the SNPs surface, indicating the presence of spherical SNPs. The inter-particle distance in the SNPs assemblies or aggregates decreases [35, 36].

TEM Analysis

Figure 2 shows the representative TEM image of the 3-HF/SNPs complex with the corresponding particle size

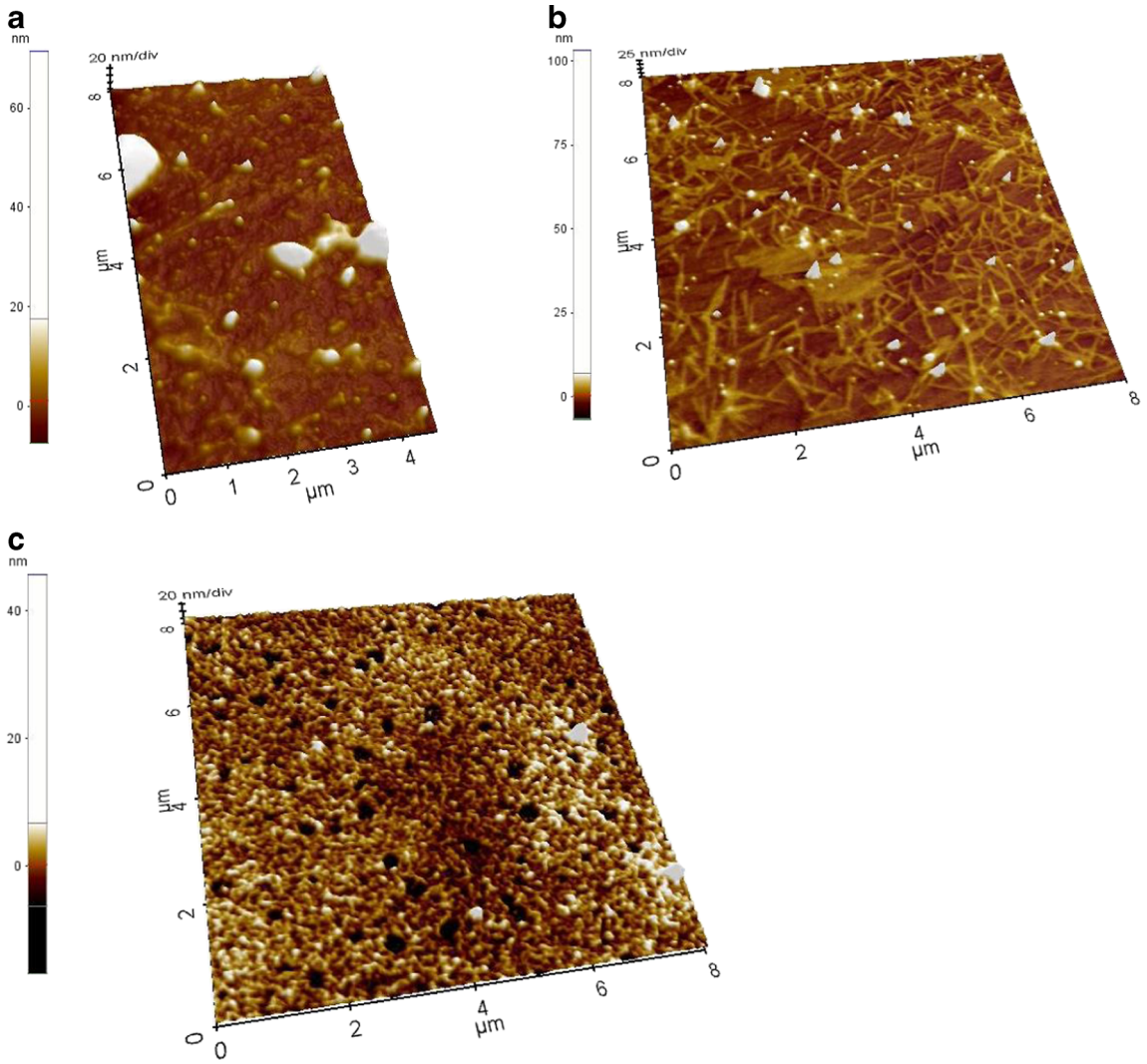

Fig. 5 3D AFM images of SNPs (**a**), 3-HF/SNPs (**b**) and 3-HF/BSA/SNPs (**c**) with 3-HF: BSA=10:1

distribution of SNPs. As can be seen, individual particles of spherical shape were mostly observed, and their mean size was about 7.8 nm, in line with the plasmon band resonance in Fig. 1. Thus, the presence of 3-HF leads to Ag nanoparticle size slightly smaller than the one of the bare SNPs (~9 nm) [35] and in the presence of another type of flavonoid compound, riboflavin, the size is ~10 nm [36]. Given the NPs diameter of ~9 nm and based on their plasmon band resonance in Fig. 1, we assessed the concentration of Ag nanoparticles to 0.9 micromolar. Note also that the lack of close contact among the nanoparticles supports the steric stabilization driven by the adsorbed 3-HF.

Fluorescence Measurements

To have more insights on the behavior of 3-HF in a SNPs/BSA complex, especially on the 3-HF-BSA binding in a SNPs complex, Fig. 3a presents the fluorescence emission spectra of 3-HF in the absence and in the presence of BSA, in a SNPs complex, at an excitation wavelength of 365 nm. 3-HF is weakly fluorescent in SNPs complex with the emission wavelength, λ_{em}=520 nm, characteristic to Tautomer (T^*) form and a shoulder at ~478 nm appears, attributed to the anion (A^*) form of 3-HF. In the presence of BSA protein, an increase in the fluorescence emission of 3-HF is observed with the appearance of two well structured emission bands: at λ_{em}= 520 nm, from T^* form and at λ_{em}=478 nm, from A^* form of 3-HF. The emission of both A^* and T^* forms increases as the concentration of BSA increases, without any shifted emission wavelengths. This feature is due to the surrounding environment of 3-HF, especially due to H-bonding. Thus, 3-HF binds to BSA and than the complex is adsorbed on SNPs surface. The binding constant (K) between 3-HF and BSA in a SNPs complex can be estimated from the fluorescence emission data by using the modified Benesi-Hildebrand equation, such as [37]:

$$1/\Delta F = 1/\Delta F_{max} K[BSA] + 1/\Delta F_{max}$$

with $\Delta F = F_x - F_0$, F_x and F_0 represent the fluorescence intensities of T^* form of the 3-HF in the presence and absence of total added BSA, respectively. ΔF_{max} is the maximum change in the fluorescence T^* form intensity and K is the binding constant. The variation $1/\Delta F$ of the 3-HF tautomer fluorescence intensity vs. 1/[BSA] shows a good linearity

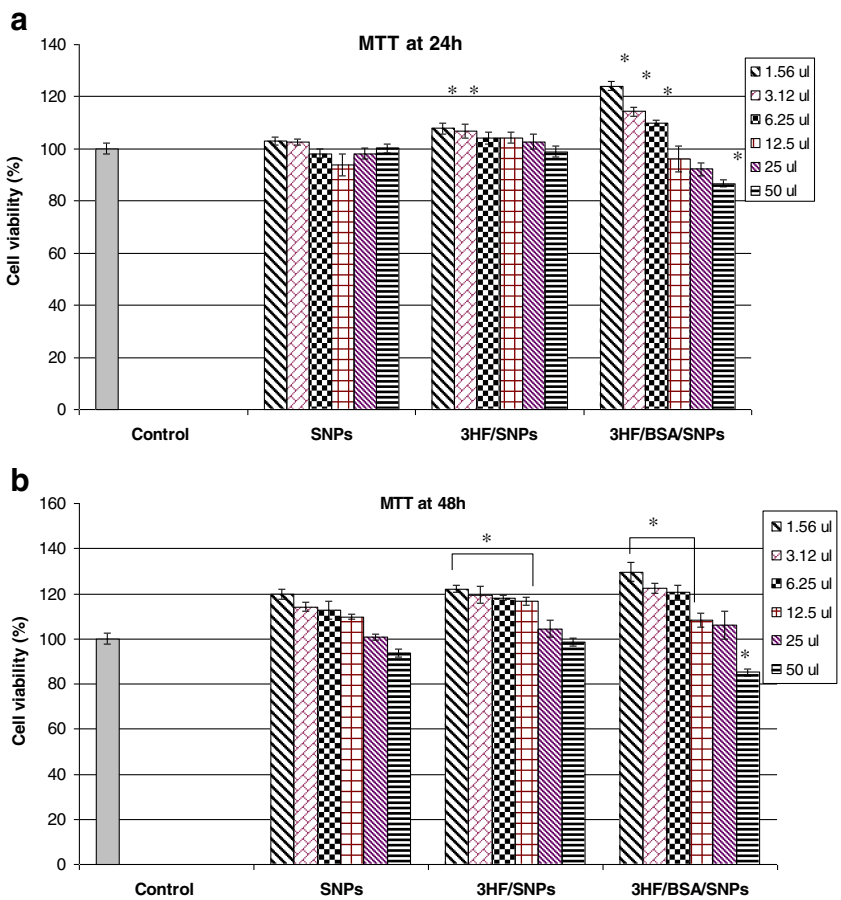

Fig. 6 Viability of L929 mouse fibroblast cells cultivated in the presence of different concentrations (1.56 μl; 3.12 μl; 6.25 μl; 12.5 μl; 25 μl; 50 μl) of SNPs, 3-HF/SNPs, 3-HF/BSA/SNPs, for 24 h (**a**) and 48 h (**b**), assessed by MTT assay. *Error bars* represent mean±SD, for n= 3. *p<0.05, compared to the untreated cells (control), considered 100 % viable

which indicates that the 3-HF is binding BSA with the K value, $K=1.71\times10^{4}$ M^{-1} (SE=4.67×10^{-4}, $r^2=0.997$). Thus, a good affinity of 3-HF towards BSA, on SNPs is observed. Figure 3b shows the fluorescence excitation spectra, monitored at 530 nm, of 3-HF with and without BSA, on SNPs in direct comparison with an aqueous solution of 3-HF. Significant changes are observed as follows: for 3-HF/BSA/SNPs system, a broad band at ~429 nm is noticed, corresponding to the anionic form of 3-HF. A shoulder at ~322 nm appears from the neutral form of 3-HF. Without BSA, the emission bands that appeared at 311 and 345 nm correspond to the neutral form of 3-HF, while its anionic form appears in this case at ~416 nm. The fluorescence excitation spectrum of an aqueous solution of 3-HF reveals the bands at 308 and 348 nm which correspond to the absorption of neutral form of 3-HF and no anionic form was detected. On SNPs, a broad band corresponding to the absorption of Trp^{212}, at ~284 nm, is observed therefore slight perturbation at the binding site of the BSA appears on SNPs. In these lines, Fig. 4 shows the Trp^{212} fluorescence emission of the 3-HF/BSA/SNPs system at an excitation wavelength of 280 nm. As can be observed, a strong blue-shift fluorescence emission of BSA (λ_{em}=326 nm) is noticed as compared with a free BSA, (λ_{em}=338 nm). Thus, a protective effect of BSA structure when 3-HF binds to BSA and than is adsorbed on SNPs, with a more hydrophobic environment of Trp^{212}, is considered.

AFM Measurements

In order to get insights on the surface morphology of SNPs at 3-HF/BSA adsorption, Fig. 5 presents the AFM image of SNPs (Fig. 5a), of 3-HF/SNPs (Fig. 5b) and of 3-HF/BSA/SNPs (Fig. 5c) at a molar ratio 3-HF: BSA=10:1. It appears that, Fig. 5c, BSA-binding to SNPs in a "side-on" binding, in which end-on binding results in a higher surface coverage of BSA on the SNPs surface. The results indicate a cross-linking or electrostatic forces that leads to a spontaneously attachement of the BSA protein to the SNPs surface.

Evaluation of In Vitro Cytotoxicity

Complementary information on in vitro cytotoxicity of tested SNPs systems was obtained from a quantitative determination of cell viability by MTT assay and a qualitative evaluation of cell morphology by light microscopy in L929 cell line. The viability of fibroblasts

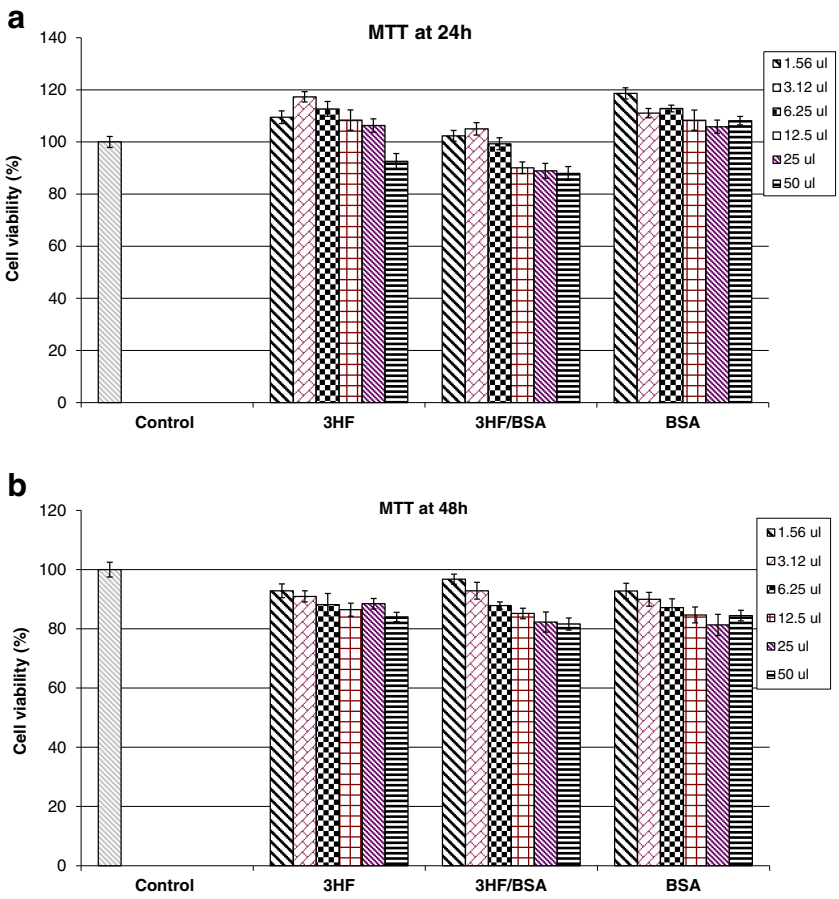

Fig. 7 Viability of L929 mouse fibroblast cells cultivated in the presence of different concentrations (1.56 µl; 3.12 µl; 6.25 µl; 12.5 µl; 25 µl; 50 µl) of 3-HF, 3-HF/BSA, BSA, for 24 h (**a**) and 48 h (**b**), assessed by MTT assay. *Error bars* represent mean ±SD, for $n=3$

cultivated in the presence of SNPs (0.9 μM), 3-HF (1.2×10^{-4} M)/SNPs and 3-HF (1.2×10^{-4} M)/BSA (2.06 μM)/SNPs (0.9 μM) is presented in Fig. 6. Different volumes from each reaction mixture were tested vs. time, at 24 h (Fig. 6a) and 48 h (Fig. 6b), respectively. The analysis of recorded data showed that cell viability values ranged between 85.1 and 129.59 % for all tested nanoproducts. These viability values higher than 80 % indicated that all samples had no cytotoxicity at any of the tested concentrations, after 24 and 48 h of cultivation in L929 fibroblast cell culture. After 24 h of cultivation, the systems containing 3-HF (3HF/SNPs and 3-HF/BSA/SNPs) presented values of cell viability (104.16–124.12 %) significantly ($p<0.05$) higher than control (100 %), at doses of 1.56÷6.25 μl (Fig. 6a). After 48 h of cultivation, in the same range of concentrations, the cell viability values varied between 118.16 and 129.59 % (Fig. 6b). These results demonstrated that samples containing 3HF presented an effect of mitochondrial metabolism stimulation in L929 fibroblast cell culture. To better compare, Fig. 7a and b show the viability of fibroblast cells cultivated in the presence of the same doses (1.56÷50 μl) of SNPs, 3-HF/SNPs and 3-HF/BSA/SNPs, for 24 h (Fig. 7a) and for 48 h (Fig. 7b). As can be observed the samples are not cytotoxic (they have a viability of over 80 %) but the cell viability decreased at 48 h compared to 24 h. Thus when they were encapsulated in nanoparticles, the cell viability increased at 48 h compared to 24 h. That means the encapsulation favors the overtaking of the substance in the cells (intracytoplasmatic) and the 3-HF has a positive influence on the cell metabolism.

In the case of the 3-HF/BSA/SNPs system cultured at low dose (1.56 μl) with fibroblast cells, the highest values of cell viability were registered, 124.12 % at 24 h of cultivation and 129.59 % at 48 h of cultivation (Fig. 8a). These values were significantly ($p<0.05$) higher than those of nanosystems without BSA (3-HF/SNPs and SNPs systems). In direct comparison, Figure 8b presents the 3-HF/BSA system cultured, in the same dose (1.56 μl) with fibroblast cells. Overall, 3-HF/BSA/SNPs system was the most biocompatible, for both periods of cultivation in doses up to 6.25 μl.

Figure 9 presented comparative light micrographs of L929 fibroblast cells cultivated in the presence of different concentrations of nanosystems, for 48 h. No morphological changes of cell membranes, cytoplasm or nuclei were observed at any tested concentration of samples. The images showed that treated cells maintained their normal spindle-shaped aspect, characteristic for fibroblasts, with euchromatic nuclei with 1–2 nucleoli and a clear cytoplasm, similar to untreated cells (control) and with 3-HF (50 μl). The cell density varied with

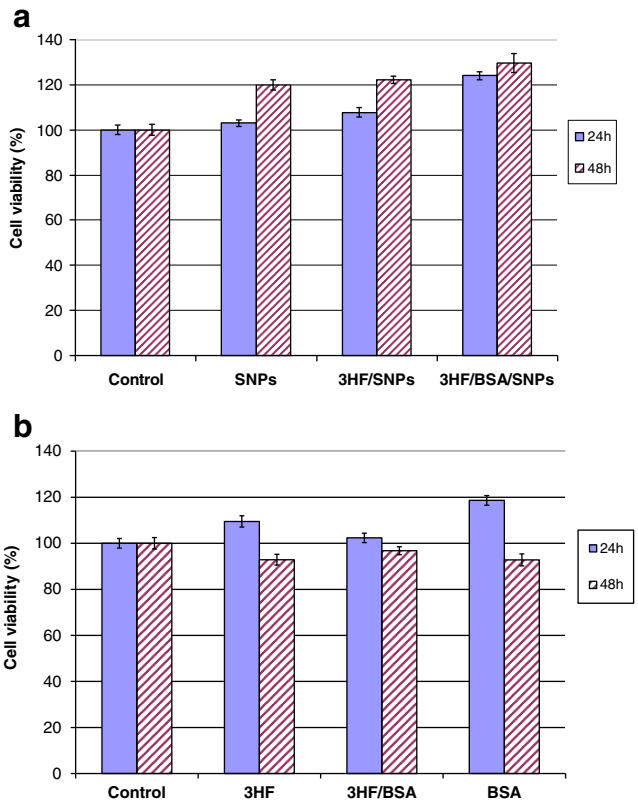

Fig. 8 Viability of L929 mouse fibroblast cells cultivated in the presence of 1.56 μl of SNPs, 3-HF/SNPs, 3-HF/BSA/SNPs, for 24 and 48 h (**a**), and in the presence of 1.56 μl of 3-HF, 3-HF/BSA, BSA (**b**) assessed by MTT assay. *Error bars* represent mean±SD, for $n=3$

sample concentration, at low doses being similar to the control and reaching an almost complete monolayer (85–92 %), after 48 h of cultivation (Fig. 9a, c, e). At higher doses of reaction mixture (50 μl), the cell density was lower (Fig. 9b, d, f).

All these results demonstrated that all nanosystems tested in L929 fibroblast cells were not cytotoxic.

Conclusions

Analyzing the results, the following conclusions may be pointed out:

The size of the SNPs when 3-HF binds to BSA and than is adsorbed on SNPs surface was found to be ~7.79 nm;
In the 3-HF/BSA/SNPs systems, strong fluorescence emission was observed from both 3-HF forms: the anion form (λ_{em}=478 nm) and tautomer form (λ_{em}=520 nm); a protective effect of BSA structure when 3-HF (in its anion form) binds to BSA and than is adsorbed on SNPs, with a more hydrophobic environment of tryptophan, Trp^{212}, was shown;
Cell viability values determined by MTT assay for mouse fibroblasts cultivated in the presence of SNPs, 3HF/SNPs

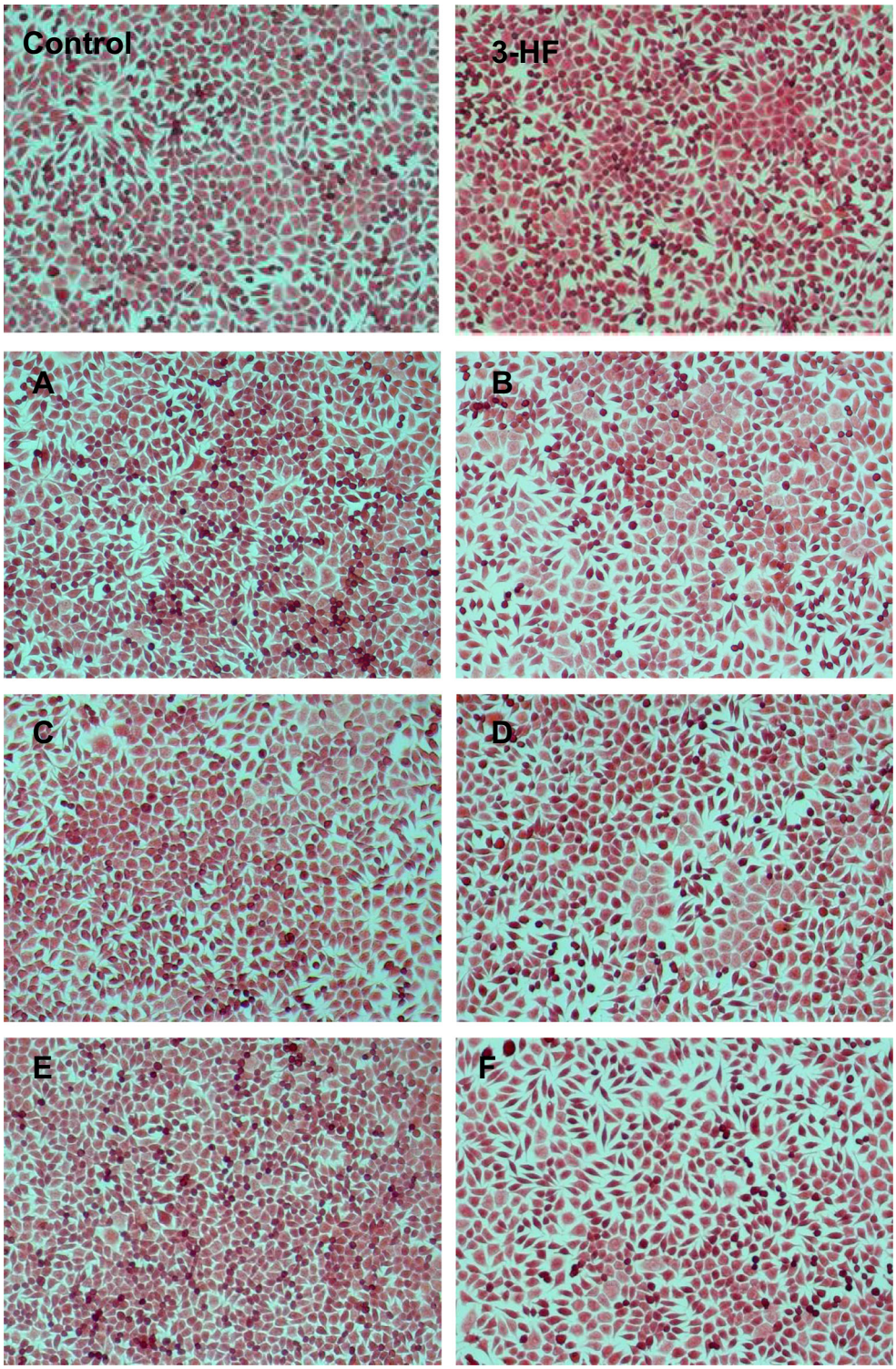

Fig. 9 Light micrographs of L929 fibroblast cells cultivated for 48 h in the presence of SNPs, 1.56 μl (**a**), and 50 μl (**b**); 3HF/SNPs, 1.56 μl (**c**) and 50 μl (**d**); 3HF/BSA/SNPs, 1.56 μl (**e**) and 50 μl (**f**). (H&E staining, 10×)

and 3-HF (120 μM)/BSA (2.06 μM)/SNPs (0.9 μM) indicated that all tested volumes of the reaction mixture were not cytotoxic;

Fibroblasts cultivated in direct contact with 3-HF (120 μM)/BSA (2.06 μM)/SNPs (0.9 μM) presented the highest degree of biocompatibility at low concentrations range, 1.56÷6.25 μl of reaction mixture;

Light microscopy images showed a normal cell morphology, similar to untreated cells, after 48 h of cultivation, for all tested nanosystems concentrations;

We can envision that expanding applications of 3-HF/BSA/SNPs, in the above tested concentrations, offers great promise for treatment of oxidative stress concerning cell viability.

Acknowledgments This work was supported by a grant of the Romanian National Authority for Scientific Research, CNCS – UEFISCDI, project number PN-II-RU-TE-2012-3-0055.

References

1. Rusznyak S, Szent-Gyorgi A (1936) Vitamin P: flavonols as vitamins. Nature 138:27. doi:10.1038/138027a0
2. Takahama U (1983) Suppression of photoperoxidation by quercetin and its glycosides in spinach chloroplast. Photochem Photobiol 38: 363–367
3. Harborne JB (1988) In: Cody V, Middleton E, Harborne JB, Beretz A (eds) Flavonoids in the environment: structure-activity relationship. Alan R. Liss, New York
4. Lamson DW, Brignall MS (2000) Antioxidants and cancer III: quercetin. Altern Med Rev 5:196–208
5. William RJ, Spencer JS, Rice-Evans C (2004) Flavonoids: antioxidants or signalling molecules? Free Radic Biol Med 36:838–849
6. Anderson OM, Markham KR (2006) Flavonoids: chemistry, biochemistry and applications. CRC Press, Boca Raton
7. Sengupta PK, Kasha M (1979) Excited state proton- transfer spectroscopy of 3-hydroxyflavone and quercetin. Chem Phys Lett 68: 382–385
8. Wolfbeis OS (1985) In: Schulman SG (ed) Molecular luminescence spectroscopy: methods and applications part I. Wiley, New York
9. Guharay J, Sengupta B, Sengupta PK (2001) Proteins 43:75
10. Demchenko AP, Ercelen S, Roshal AD, Klymchenko AS (2002) Pol J Chem 76:1287
11. Sytnik A, Gormin D, Kasha M (1994) Interplay between excited-state intramolecular proton transfer and charge transfer in flavonols and their use as protein-binding-site fluorescence probes. Proc Natl Acad Sci U S A 91:11968–11972
12. Sytnik A, Litvinyuk I (1996) Energy transfer to a proton-transfer fluorescence probe: tryptophan to a flavonol in human serum albumin. Proc Natl Acad Sci U S A 93:12959–12963
13. Hussain S, Ferguson C (2006) Best evidence topic report. Silver sulphadiazine cream in burns. Emerg Med J 23:929–932
14. Bhattacharya R, Mukherjee P (2008) Biological properties of "naked" metal nanoparticles. Adv Drug Deliv Rev 60:1289–1306
15. Muangman P, Muangman S, Opasanon S, Keorochana K, Chuntrasakul C (2009) Benefit of hydrocolloid SSD dressing in the outpatient management of partial thickness burns. J Med Assoc Thai 92:1300–1305
16. Caruso DM, Foster KN, Blome-Eberwein SA, Twomey JA, Herndon DN, Luterman A, Silverstein P, Antimarino JR, Bauer GJ (2006) Randomized clinical study of hydrofiber dresssing with silver or silver sulphadiazine in the management of partial thickness burns. J Burn Care Res 27:298–309
17. Pearce ME, Melanko JB, Salem AK (2007) Multifunctional nanorods for biomedical applications. Pharm Res 24:2335–2352
18. Xiao Y, Gao X (2010) Use of IgY antibodies and semiconductor nanocrystal detection in cancer biomarker quantitation. Biomark Med 4:227–239
19. Shrivastava S, Bera T, Roy A, Singh G, Ramachandrarao P, Dash D (2007) Characterization of enhanced antibacterial effects of novel silver nanoparticles. Nanotechnology 18:225103–225112
20. Uygur F, Oncul O, Evinc R, Diktas H, Acar A, Ulkur E (2009) Effects of three different topical antibacterial dressings on Acinetobacter baumannii-contaminated full-thickness burns in rats. Burns 35:270–273
21. Muthu MS, Wilson B (2010) Multifunctional radionanomedicine. A novel platforme for effective cancer imaging and therapy. Nanomedicine 5:169–171
22. Su Y, Qiao S, Yang H, Yang C, Jin Y, Stahr F, Sheng J, Cheng L, Ling C, Lu GQ (2010) Titanate-silica mesostructured nanocables: synthesis, structural analysis and biomedical applications. Nanotechnology 21:065604. doi:10.1088/0957-4484/21/6/065604
23. Sondy I, Salopek-Sondi B (2004) Silver nanoparticles as antimicrobial agent: a case study on *E. Coli* as a model for Gram-negative bacteria. J Colloid Interface Sci 275:177–182
24. Kim JS, Kuk E, Nam Yu K et al (2007) Antimicrobial effects of silver nanoparticles. Nanomed Nanotechnol Biol Med 3:95–101
25. Wei D et al (2009) The sysnthesis of chitosan-based siver nanoparticles and their antibacterial activity. Carbohydr Res 344:2375–2382
26. Rai M, Yadav A, Gade A (2009) Silver nanoparticles as a new generation of antimicrobials. Biotechnol Adv 27:76–83
27. Guzman MG, Dille J, Godet S (2009) Synthesis of silver nanoparticles by chemical reduction method and their antibacterial activity. Int J Chem Biol Eng 2–3:104–111
28. Wong KKY, Liu X (2010) Silver nanoparticles—the real "silver bullet" in clinical medicine? Med Chem Commun 1:125–131
29. De Lima R, Seabra AB, Duran N (2012) Silver nanoparticles: a brief review of cytotoxicity and genotoxicity of chemically and biogenically synthesized nanioparticles. J Appl Toxicol 32:867–879
30. Manke A, Wang L, Rojanasakul Y (2013) Mechanisms of nanoparticles—induced oxidative stress and toxicity. BioMed Res Int. doi: 10.1155/2013/942916
31. Matsuo M, Sasaki N, Saga K, Kaneko T (2005) Cytotoxicity of flavonoids towards cultured normal human cells. Biol Pharm Bull 28:253–259
32. Voicescu M, Nistor CL, Meghea A (2015) Insights into the antioxidant activity of some flavones on silver nanoparticles using a chemiluminescence method. J Lumin 157:243–248. doi:10.1016/j.jlumin.2014.08.058
33. Angelescu DG, Vasilescu M, Somoghi R, Donescu D, Teodorescu VT (2010) Kinetics and optical properties of the silver nanoparticles in aqueous L64 block copolymer solutions. Colloids Surf A Physicochem Eng Asp 366:155–162
34. Craciunescu O, Moldovan M, Moisei M, Trif M (2013) Liposomal formulation of chondroitin sulfate enhances its antioxidant and anti-inflammatory potential in L929 fibroblast cell line. J Liposome Res 23:145–153
35. Voicescu M, Ionescu S, Angelescu DG (2012) Spectroscopic and coarse-grained simulation studies of the BSA and HSA protein adsorption on silver nanoparticles. J Nanoparticle Res 14:1174. doi:10.1007/s11051-012-1174-0
36. Voicescu M, Angelescu DG, Ionescu S, Teodorescu VS (2013) Spectroscopic analysis of the riboflavin—serum albumins interaction on silver nanoparticles. J Nanoparticle Res 15:1555. doi:10.1007/s11051-013-1555-z
37. Benesi HA, Hildebrand JH (1949) A spectrophotometric investigation of the interaction of iodine with aromatic hydrocarbons. J Am Chem Soc 71:2703–2707